

RESEARCH ARTICLE

Computational Modeling Reveals Key Contributions of KCNQ and hERG Currents to the Malleability of Uterine Action Potentials Underpinning Labor

Wing-Chiu Tong¹, Rachel M. Tribe², Roger Smith³, Michael J. Taggart^{1*}

1. Institute of Cellular Medicine, Newcastle University, Newcastle upon Tyne, United Kingdom, 2. Division of Women's Health, King's College London and King's Health Partners, London, United Kingdom, 3. Hunter Medical Research Institute, University of Newcastle, New Lambton, New South Wales, Australia

*michael.taggart@ncl.ac.uk



 OPEN ACCESS

Citation: Tong W-C, Tribe RM, Smith R, Taggart MJ (2014) Computational Modeling Reveals Key Contributions of KCNQ and hERG Currents to the Malleability of Uterine Action Potentials Underpinning Labor. PLoS ONE 9(12): e114034. doi:10.1371/journal.pone.0114034

Editor: Roger C. Young, University of Tennessee Health Science Center, United States of America

Received: June 18, 2014

Accepted: November 3, 2014

Published: December 4, 2014

Copyright: © 2014 Tong et al. This is an open-access article distributed under the terms of the [Creative Commons Attribution License](https://creativecommons.org/licenses/by/4.0/), which permits unrestricted use, distribution, and reproduction in any medium, provided the original author and source are credited.

Data Availability: The authors confirm that all data underlying the findings are fully available without restriction. All relevant data are within the paper and its Supporting Information files.

Funding: This work was supported by the UK Medical Research Council (G0900525, G1100243, www.mrc.ac.uk) including a Bioinformatics Training Fellowship to WCT (G0902091). The funder had no role in study design, data collection and analysis, decision to publish, or preparation of the manuscript.

Competing Interests: The authors have declared that no competing interests exist.

Abstract

The electrical excitability of uterine smooth muscle cells is a key determinant of the contraction of the organ during labor and is manifested by spontaneous, periodic action potentials (APs). Near the end of term, APs vary in shape and size reflecting an ability to change the frequency, duration and amplitude of uterine contractions. A recent mathematical model quantified several ionic features of the electrical excitability in uterine smooth muscle cells. It replicated many of the experimentally recorded uterine AP configurations but its limitations were evident when trying to simulate the long-duration bursting APs characteristic of labor. A computational parameter search suggested that delayed rectifying K^+ currents could be a key model component requiring improvement to produce the longer-lasting bursting APs. Of the delayed rectifying K^+ currents family it is of interest that KCNQ and hERG channels have been reported to be gestationally regulated in the uterus. These currents exhibit features similar to the broadly defined uterine I_{K1} of the original mathematical model. We thus formulated new quantitative descriptions for several I_{KCNQ} and I_{hERG} . Incorporation of these currents into the uterine cell model enabled simulations of the long-lasting bursting APs. Moreover, we used this modified model to simulate the effects of different contributions of I_{KCNQ} and I_{hERG} on AP form. Our findings suggest that the alterations in expression of hERG and KCNQ channels can potentially provide a mechanism for fine tuning of AP forms that lends a malleability for changing between plateau-like and long-lasting bursting-type APs as uterine cells prepare for parturition.

Introduction

The timely onset and maintenance of regular contractions of the uterus are necessary features for ensuring successful parturition and safe delivery of a baby and placenta. These contractions are driven by episodic, spontaneous myogenic action potentials (APs) that exhibit a broad spectrum of form and duration, the variability of which is likely to be beneficial in facilitating the co-ordination of uterine contractile effort during labor. For example, as pregnancy progresses uterine APs become more frequent and regular, the duration of the APs progressively lengthens [1] and they are often manifested as bursting APs that can last for many seconds to minutes [2], thus contributing to a greater time-averaged force of uterine contractions at parturition. Although more frequently shown in the recordings of multi-cellular uterine tissues, these APs have also been reported in single uterine smooth muscle (myometrial) cells isolated from near-labor, and in-labor, animals and humans [2, 3]. The quest for a deeper understanding of the mechanisms that regulate these changes in uterine AP forms would benefit from computational biology approaches. A recently established mathematical model for uterine smooth muscle cell (USMC) electrical excitability is a useful starting point for these considerations [4]. The electrogenic components of this model were largely based on published data from uterine and other smooth muscles. These components were validated by experimental data and the model reproduced several published types of AP forms (spike, plateau and short bursts of spikes) of variable duration $\approx 0.5 - 10$ secs. However, despite showing these positive simulation performances, this model was limited in its ability to computationally reproduce all uterine AP behaviors, in particular, the very long duration (tens of sec to mins) bursting-type APs that have been experimentally noted in uterine smooth muscle cells from late pregnancy [1–3]. Also, another related problem is that the membrane voltage failed to repolarize upon cessation of the stimulation when it had remained at a depolarized level for too long, such as during attempts to simulate a prolonged AP. These limitations restrict the use of the cell model to simulating uterine AP responses of shorter duration.

Our aims in this study, therefore, were two-fold. First, to identify membrane currents that are essential for forming the characteristics of long duration bursting-type APs with full repolarization capacity that are, presently, lacking in the uterine cell model. Second, to perform simulation experiments to explore the possible mechanistic roles of these components in the malleability of uterine cell excitability.

Results and Discussion

Insight from one-at-a-time sensitivity measures

The original USMC model [4] (the electrogenic components are depicted in [Figure 1A](#)) reliably simulated uterine bursting-type and plateau-type APs of short duration, examples of which are given in [Figure 1B-C](#). However, to computationally

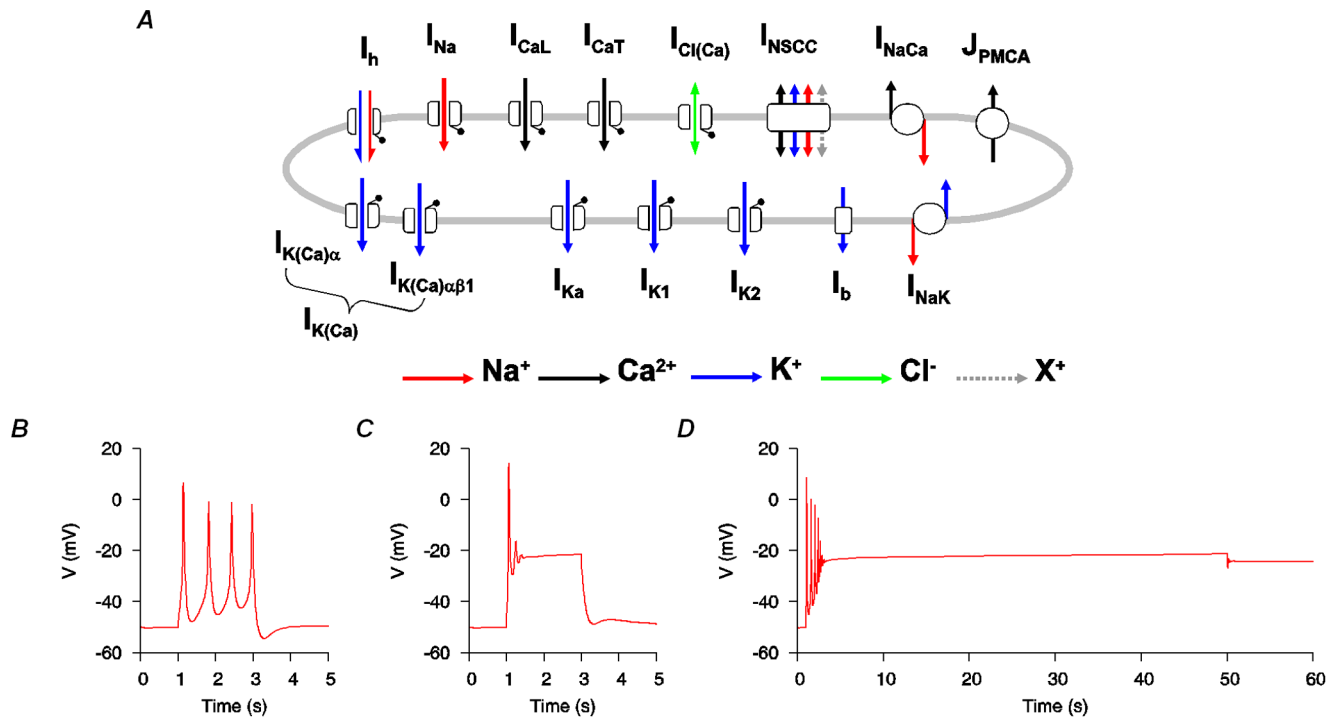


Figure 1. Electrogenic components of the initial USMC model. A, Schematic representation of the 14 ion channels/exchangers that contributed to the initial USMC model of myometrial electrical excitability [4]. B-D, this USMC model [4] reproduced different AP forms of short duration but it could not simulate long-lasting APs. B, short bursting-type AP evoked by a 2 s current clamp stimulus (*I*_{st}) of -0.2 pA pF^{-1} . C, short plateau-type AP evoked by a 2 s *I*_{st} of -0.5 pA pF^{-1} . D, an attempt to simulate a long duration AP with a 50 s *I*_{st} of -0.25 pA pF^{-1} resulted in a plateau-like AP that failed to repolarize at the end of the stimulus. All three simulated APs were initiated from the same initial conditions.

doi:10.1371/journal.pone.0114034.g001

reproducing APs of long duration bursting was a challenge (Figure 1D). We, therefore, performed a simple computational parameter sensitivity analysis to assess which kinetic properties would have the ability to improve the functionality of the model.

Parameters such as the maximal conductances (\bar{g}), the half activations and inactivations ($V_{0.5}$), the slope factors (k) of the steady-state activations and inactivations, and the time constant functions of activation or inactivation (τ), were changed one-at-a-time while holding the others at their fixed values. At each alteration, the influence of the parameter change on the model output was assessed by examining the form and duration of the initial burstings in a simulated AP evoked with a 50 s current clamp stimulus. The results were ranked and evaluated. We found that no single intrinsic parameter alteration of the ionic currents could produce a transition from short to long duration bursting APs. However, modification of some parameters could prolong the initial spiking period during an AP; in particular, changes in the maximal conductance (\bar{g}_{K1}) and the fast inactivation time constant (τ_{f1}) of the uterine delayed rectifying K^+ current, I_{K1} (not to be confused with the time-independent inward rectifying potassium current commonly designated also as I_{K1} in cardiac cells). Figure 2 shows the result of changing the kinetic properties of I_{K1} on the uterine AP.

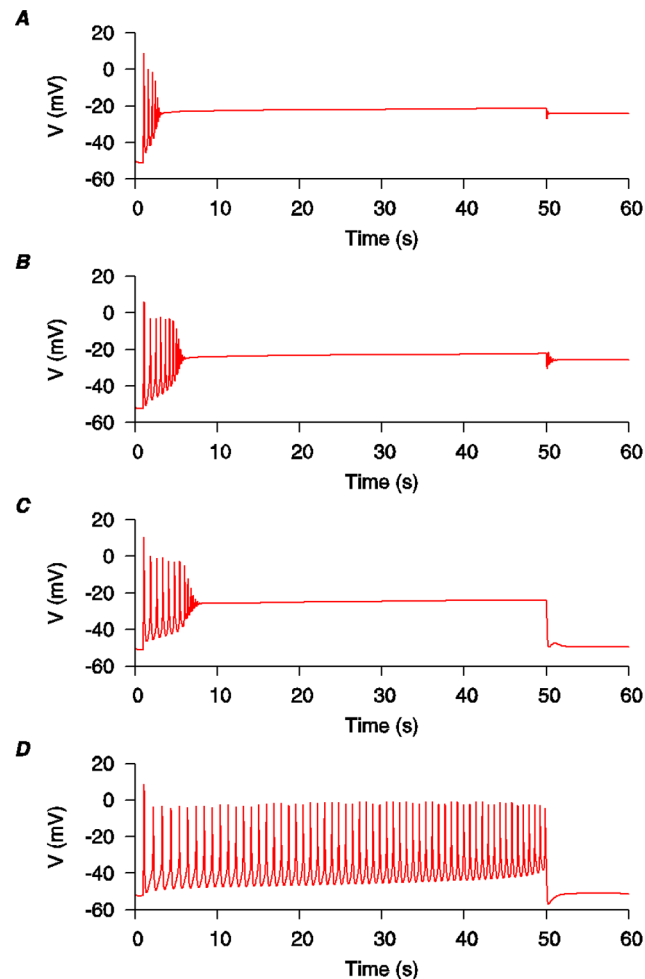


Figure 2. Altering the kinetic properties of I_{K1} in the initial USMC model was found to favor longer bursting-type APs. A, the standard configuration of the initial USMC model [4] as depicted in Figure 1D. B, increasing the I_{K1} conductance (\bar{g}_{K1} from 0.52 nS pF^{-1} to 0.64 nS pF^{-1}) prolonged the initial bursting phase a little without enabling repolarization of the AP. C, alternatively, scaling the I_{K1} time constants (activation: τ_q , 2X; inactivation: τ_{r1} , 20X and τ_{r2} , 20X) also prolonged the bursting phase and facilitated the membrane voltage repolarization at the end of the stimulus. D, by changing both the conductance and time constants of I_{K1} together, the bursting persisted until the end of the stimulus and the membrane voltage repolarized on stimulus cessation.

doi:10.1371/journal.pone.0114034.g002

Compared to the control case (Figure 2A), the initial bursting duration was slightly increased when \bar{g}_{K1} was increased (Figure 2B). A similar result was obtained when τ_{r1} was scaled up but there were no apparent changes when either the activation time constant (τ_q) or the slow inactivation time constant (τ_{r2}) of I_{K1} was changed. Since all these parameters influence the same ionic current, I_{K1} , their combined influences could exert more noticeable changes on the AP form than changing one parameter in isolation. Thus, we examined the effect of I_{K1} having overall slower dynamics (τ_q , 2X; τ_{r1} , 20X; τ_{r2} , 20X) but this only slightly prolonged the initial bursting duration (Figure 2C). However, when an overall slower I_{K1} was combined with a larger conductance then the bursting continued until the end of

the stimulus (Figure 2D). The resultant AP resembled the experimentally recorded long bursting behaviors [1, 2]. This simple parameter analysis provided an insight that, in order to simulate the long-lasting bursting APs, the uterine cell model required larger and slower delayed rectifying K^+ currents. To make such changes we needed to either describe a known mechanism for causing such changes in uterine I_{K1} or replace the uterine I_{K1} with other molecularly identified K^+ currents with such biophysical properties. There is no experimental information to support the former, and so we proceeded with the latter.

Uterine whole-cell voltage-gated K^+ currents have only been roughly categorized based on their inactivation properties and their sensitivity to different broad-spectrum potassium channel blockers. For example, the uterine I_{K1} has been described as a prominent voltage-gated, delayed rectifying K^+ current rather loosely identified by its pharmacological profile and activation/inactivation dynamics [5]. Under voltage-clamp conditions, the activation threshold where I_{K1} first appears is between -60 mV to -40 mV, it has a half activation of ≈ 1.2 mV and a half-inactivation of ≈ -65 mV. The dynamics of I_{K1} are slow and the decay of the current can take as much as 10 secs. Also, I_{K1} is sensitive to 10 mM TEA but insensitive to 5 mM 4-AP. Given these rather broad characterizations, there are contributions to this current that are likely to come from a number of molecularly distinct channels. When considering the possible identity of these channels we noted the following:

(i) In rat uteri at late pregnancy mRNA encoding a very slowly activating K^+ channel increased in expression. This K^+ current shares similarities to the cardiac delayed rectifying currents I_{Ks} and I_{Kr} [6, 7].

(ii) The delayed rectifying cardiac I_{Ks} consists of the KCNQ voltage-gated pore-forming channel(s) and KCNE subunits and recent evidence suggests that uterine transcripts encoding KCNQ and KCNE subunits are gestationally regulated [8].

(iii) KCNQ activation time constants and conductances are subject to modulation by the pattern of KCNE subunit co-expression [9].

(iv) KCNQ potassium channels can be blocked by XE991 and XE991-sensitive currents in portal venous smooth muscle showed broadly similar characteristics as uterine smooth muscle I_{K1} with a half-activation of 7 mV and a half-inactivation of -54 mV; the activation threshold is -30 mV [10].

(v) KCNQ currents have pharmacological profiles similar to I_{K1} as many members of the KCNQ channels are sensitive to TEA and insensitive to 4-AP [11, 12].

(vi) A major contributor to the delayed rectifying cardiac I_{Kr} is the human *Ether-à-Go-Go*-related (hERG) channel current. Recent evidence has shown that hERG channel subunits are expressed in uterine cells and the currents sensitive to hERG inhibitors, e.g. E4031 or dofetilide, are functionally suppressed at late pregnancy [13, 14].

(vii) The dynamics of hERG currents are comparable to I_{K1} : the activation threshold is -50 mV [15, 16]; a half-inactivation is between -94 mV and -48 mV [15–18] and, depending on the recording conditions, the half-activation of hERG varies between -31 mV to 17 mV [15–21].

These data, together with the results of the parameter analysis, led us to speculate that KCNQ and hERG currents may form part of the uterine I_{K1} current. Our next task was therefore to assess how best to incorporate this experimental information into the USMC model. However, there are no experimental measurements specific to uterine smooth muscle cells on the dynamics of KCNQ currents and there is only limited information about hERG-like currents in these cells. Thus, we next sought to (i) establish quantitative descriptions of the biophysical details from clonal data for KCNQ and hERG currents and (ii) modify the USMC model by substituting I_{K1} with KCNQ and hERG currents.

Formulation of mathematical descriptions of KCNQ1, KCNQ4, KCNQ5 and hERG currents

The KCNQ subunits form the pore of K^+ channels. There are five members in the KCNQ family: Q1–Q5. In mouse uterine tissues, the mRNA expressions of all KCNQ subunits were suppressed from early to mid-gestation until late term when KCNQ1, KCNQ4 and KCNQ5 mRNA levels were increased [8]. Based on this information, we decided to formulate descriptions for currents determined by KCNQ1 (I_{KCNQ1}), KCNQ4 (I_{KCNQ4}) and KCNQ5 (I_{KCNQ5}).

There are at least three main variants of hERG protein (hERG1-3), the expressions of which impose different kinetic characteristics on the channel current. The full-length hERG (also known as hERGA or hERG1a) is found in all types of muscles cells. hERG1a is known to form a N-terminus splice variant (known as hERGb or hERG1b), which shows faster activation and deactivation, and smaller tail currents compared to hERG1a [22]. A C-terminus splice variant of hERG (also known as hERGC [19], hERG_{USO} [20] or erg-sm [16]) has also been reported, including from smooth muscle. However, the descriptions of its characteristics vary from being non-functional channels to fully conducting channels. Greenwood et al. (2009) [13] showed that both hERG1a and hERG1b, but not hERG2 or hERG3, were expressed in mouse myometrium with hERG1a being the most abundant isoform. Therefore, we developed formulations for hERG current (I_{hERG}) based upon published datasets for hERG1a.

Detailed information on the kinetics and steady-state voltage (V)-dependent parameters of I_{KCNQ} or I_{hERG} has been obtained from clonal data from heterologous expression cell systems for each channel subunit: KCNQ1 [10, 23–35], KCNQ4 [25, 30–32, 34, 36–39], KCNQ5 [31, 32, 34, 36, 38–42] and hERG [15, 16, 19, 20, 43]. Therefore, mathematical descriptions of the channel biophysical details were developed from these data. Mathematical descriptions of the biophysical characteristics of these currents are given in Appendix S1: for I_{KCNQ1} see equations 1–13; for I_{KCNQ4} see equations 14–20; for I_{KCNQ5} see equations 21–32; for I_{hERG} see equations 33–41.

The equations for I_{KCNQ1} incorporate two activation gating variables (n_{Q1f} and n_{Q1s}) and two inactivation gating variables (w_{Q1} and s_{Q1}). Steady-state values for activation and inactivation are shown in Figure 3A–B. The time constants of activation ($\tau_{n_{Q1f}}$ and $\tau_{n_{Q1s}}$) and inactivation ($\tau_{w_{Q1}}$ and $\tau_{s_{Q1}}$) are depicted in Figure 3C–D and were each obtained by fitting the raw data current tracings from

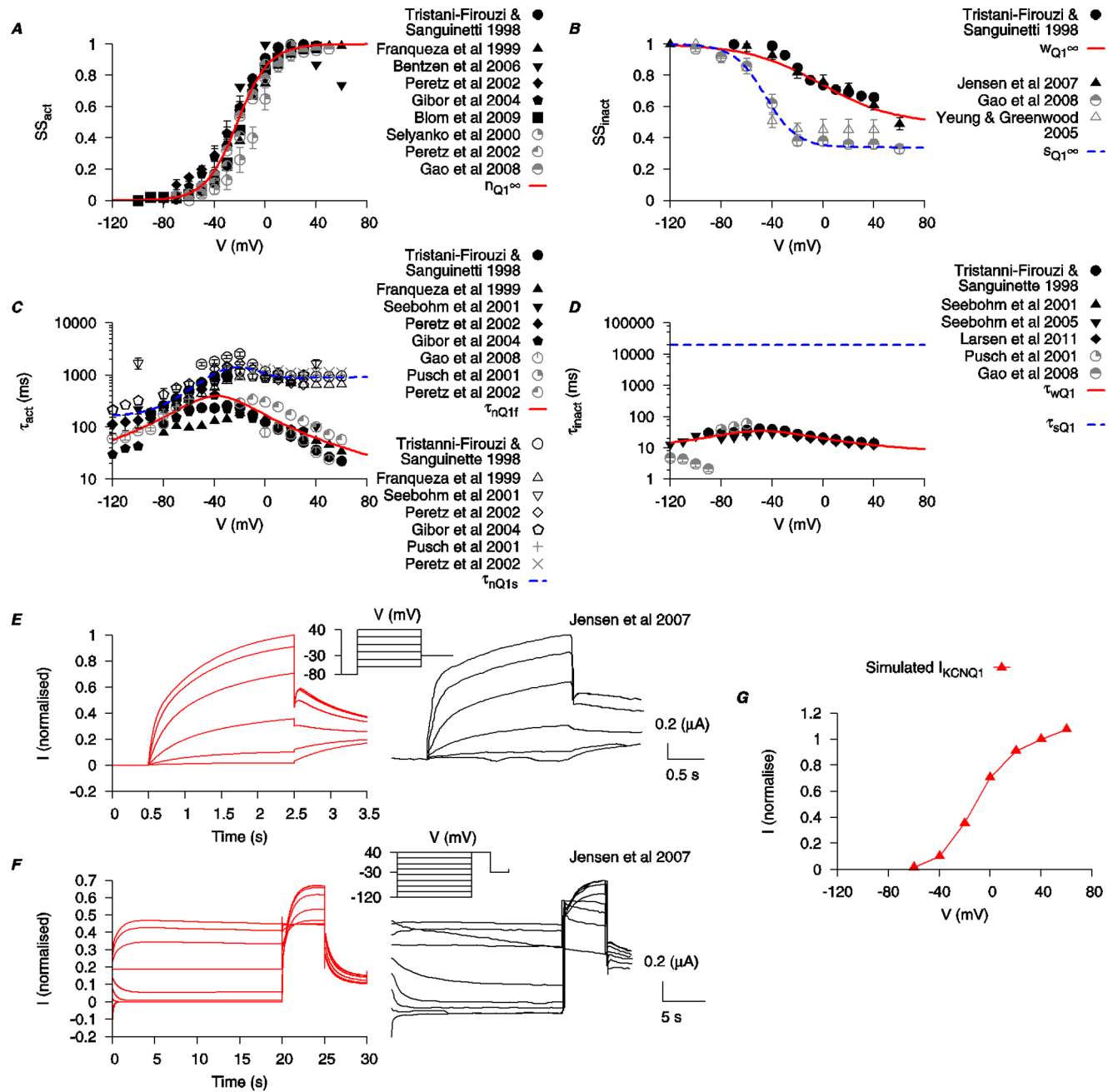


Figure 3. Biophysical characteristics of KCNQ1 current. Properties of I_{KCNQ1} were developed using experimental data from human KCNQ1 clones expressed in *Xenopus laevis* oocytes (black) and Chinese hamster cell (gray) [23–35], as well as KCNQ-like currents in mouse smooth muscle cells [10]. A, V-dependent activation steady state ($n_{Q1\infty}$). B, V-dependent steady states for fast inactivation ($w_{Q1\infty}$) and slow inactivation ($s_{Q1\infty}$). C, V-dependent activation time constants (τ_{nQ1f} and τ_{nQ1s}). D, fast (τ_{wQ1}) and slow (τ_{sQ1}) inactivation time constants. τ_{wQ1} is V-dependent and fitted to experimental data [23, 26, 27, 30, 33, 35]. τ_{sQ1} is set as a constant at 50 s. This value is chosen to best reproduce the published time tracings from Jensen et al. (2007) [32]. E and F, simulated time tracings of I_{KCNQ1} with two different voltage-clamp protocols from [32] (insets) and the experimental time tracings are shown for comparison. (Experimental tracing adapted with permission from Jensen et al. (2007); copyright 2007, Biophysical Society.) G, simulated $I-V$ relationship of I_{KCNQ1} using the same voltage-clamp protocol as in E. All $I-V$ data are normalized to the maximal current value at $V=40$ mV.

doi:10.1371/journal.pone.0114034.g003

the literature [23–35]. τ_{wQ1} is V -dependent and fitted to experimental data [23, 26, 27, 30, 33, 35]. τ_{sQ1} is set as a constant at 50 s. This value was chosen to best reproduce the published time tracings from Jensen et al. (2007) [32]. Simulated traces of I_{KCNQ1} under voltage-clamp conditions are presented in Figure 3E–F and show dynamic profiles similar to the raw data [32]. The simulated I–V relationship of I_{KCNQ1} is shown in Figure 3G.

The equations for I_{KCNQ4} incorporate an activation (n_{Q4}) and an inactivation (s_{Q4}) gating variable. Steady-state values for activation and inactivation are shown in Figure 4A–B. Blom et al. (2009) [34] reported that KCNQ4 currents were best described with a single time constant for its activation within the voltage range of –40 mV to +40 mV, and two time constants for its deactivation. Thus we used a single time constant for activation (τ_{nQ4}) and its voltage-dependency is depicted in Figure 4C. We modeled the current with one inactivation time constant (τ_{sQ4}) (Figure 4D). Raw data concerning the dynamics of inactivation of I_{KCNQ4} are limited and therefore, for simplicity, a function was chosen to fit with the data available and which best reproduced the published raw data time tracings from Jensen et al. (2007) [32]. Simulations of raw data traces of I_{KCNQ4} under voltage-clamp conditions matched well to the experimental data [32] (Figure 4E–F) and the simulated I–V relationship is shown in Figure 4G.

The equations for I_{KCNQ5} incorporate two activation gating variables (n_{Q5f} and n_{Q5s}). Steady-state values for the activation are shown in Figure 5A. The dynamics of the activation are described by two time constants (τ_{nQ5f} and τ_{nQ5s} , Figure 5C). However, it was less straightforward to mathematically describe the steady-state V -dependent inactivation of I_{KCNQ5} . For example, using functions that fitted well with the reported steady-state inactivation data of Jensen et al. (2007) [32], it was not possible to replicate the raw data current tracings from the same publication. Moreover, the hooked tail currents of I_{KCNQ5} shown in Jensen et al. (2007) [32] suggested that, in order to reproduce this feature, an inactivation faster than the activation may be required. Without sufficient other information concerning the inactivation dynamics of I_{KCNQ5} , we have, therefore, used the fast inactivation of I_{KCNQ1} and the slow inactivation of I_{KCNQ4} to represent the fast and slow inactivation conditions for I_{KCNQ5} , *i.e.*, $w_{Q5\infty} = w_{Q1\infty}$, $\tau_{wQ5} = \tau_{wQ1}$, $s_{Q5\infty} = s_{Q4\infty}$ and $\tau_{sQ5} = \tau_{sQ4}$. With these adjustments (Figure 5B,D), the simulated I_{KCNQ5} profiles were satisfactory compared to the published experimental raw data time tracings (Figure 5E–F). The simulated I–V relationship is shown in Figure 5G.

The equations for hERG incorporate two activation gating variables (h_{n1} and h_{n2}) and an inactivation gating variable (h_s). Steady-state values for activation and inactivation are shown in Figure 6A–B. The time constants of activation (τ_{hn1} and τ_{hn2}) and inactivation (τ_{hs}) are illustrated in Figure 6C–D. The kinetics of hERG currents have rather slow activation and deactivation (msec to sec) profiles but rapid inactivation (msec). As a result, the time tracings of raw data of I_{hERG} under voltage-clamp conditions often show large ‘hook’ tail currents when the command voltage is stepped down from a depolarized level. Simulations of these current tracings are shown in Figure 6E. The corresponding I–V relationships, of either the end-of-pulse current or the peak tail current, are depicted in Figure 6F.

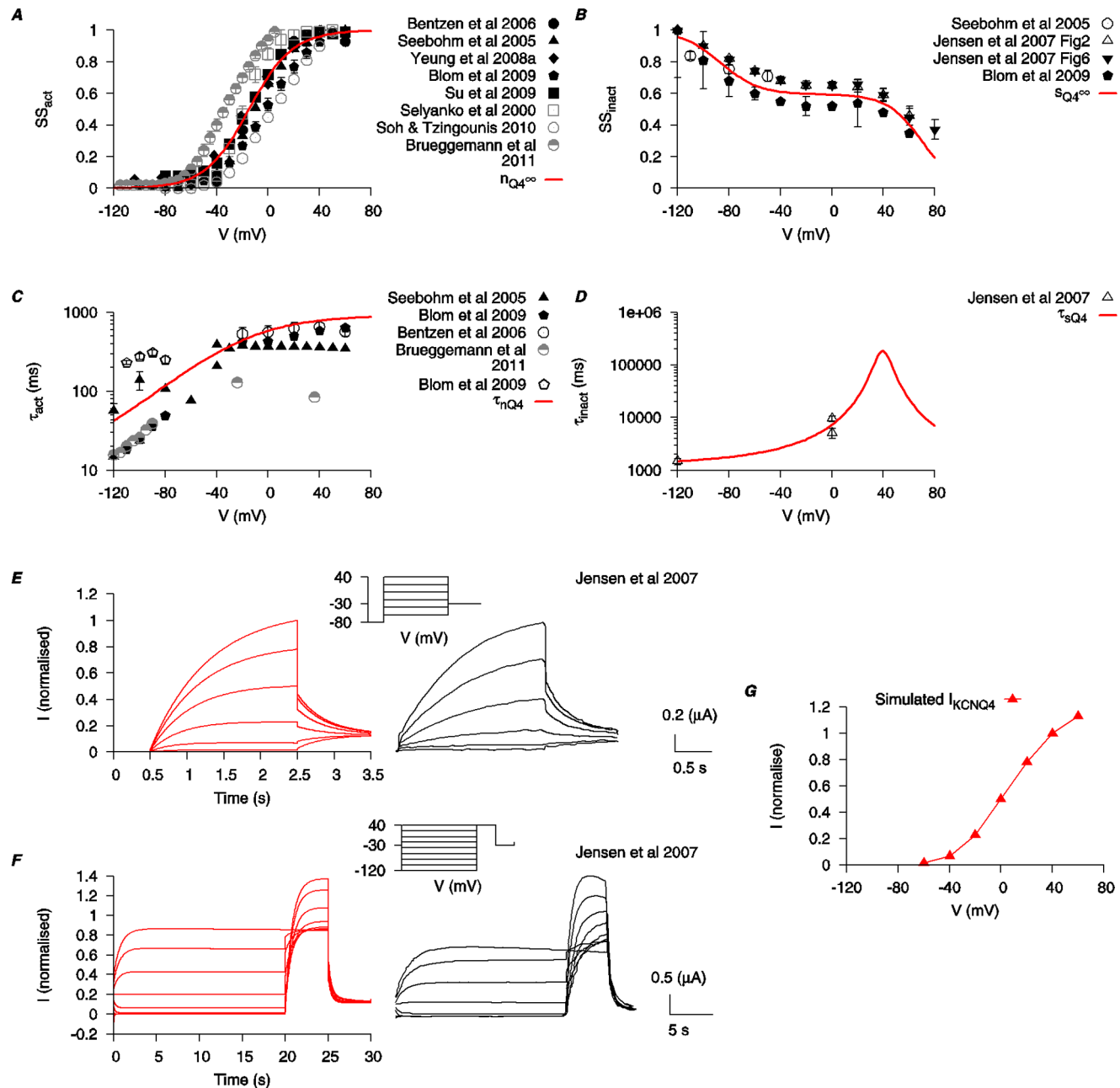


Figure 4. Biophysical characteristics of KCNQ4 current. Properties of I_{KCNQ4} are developed using experimental data from mammalian KCNQ4 clones expressed in *Xenopus laevis* oocytes (black) and other expression systems (gray) [25, 30–32, 34, 36–39]. A, V-dependent activation steady state (n_{Q4^∞}). B, V-dependent inactivation steady state (s_{Q4^∞}). C, V-dependent activation time constant (τ_{nQ4}). D, V-dependent inactivation time constant (τ_{sQ4}). E and F, simulated time tracings of I_{KCNQ4} with two different voltage-clamp protocols from Jensen et al. (2007) [32] (insets) and the experimental time tracings are shown for comparison. (Experimental tracing adapted with permission from Jensen et al. (2007); copyright 2007, Biophysical Society.) G, simulated I-V relationship of I_{KCNQ4} using the same voltage-clamp protocol as in E. All I-V data are normalized to the maximal current value at $V=40$ mV.

doi:10.1371/journal.pone.0114034.g004

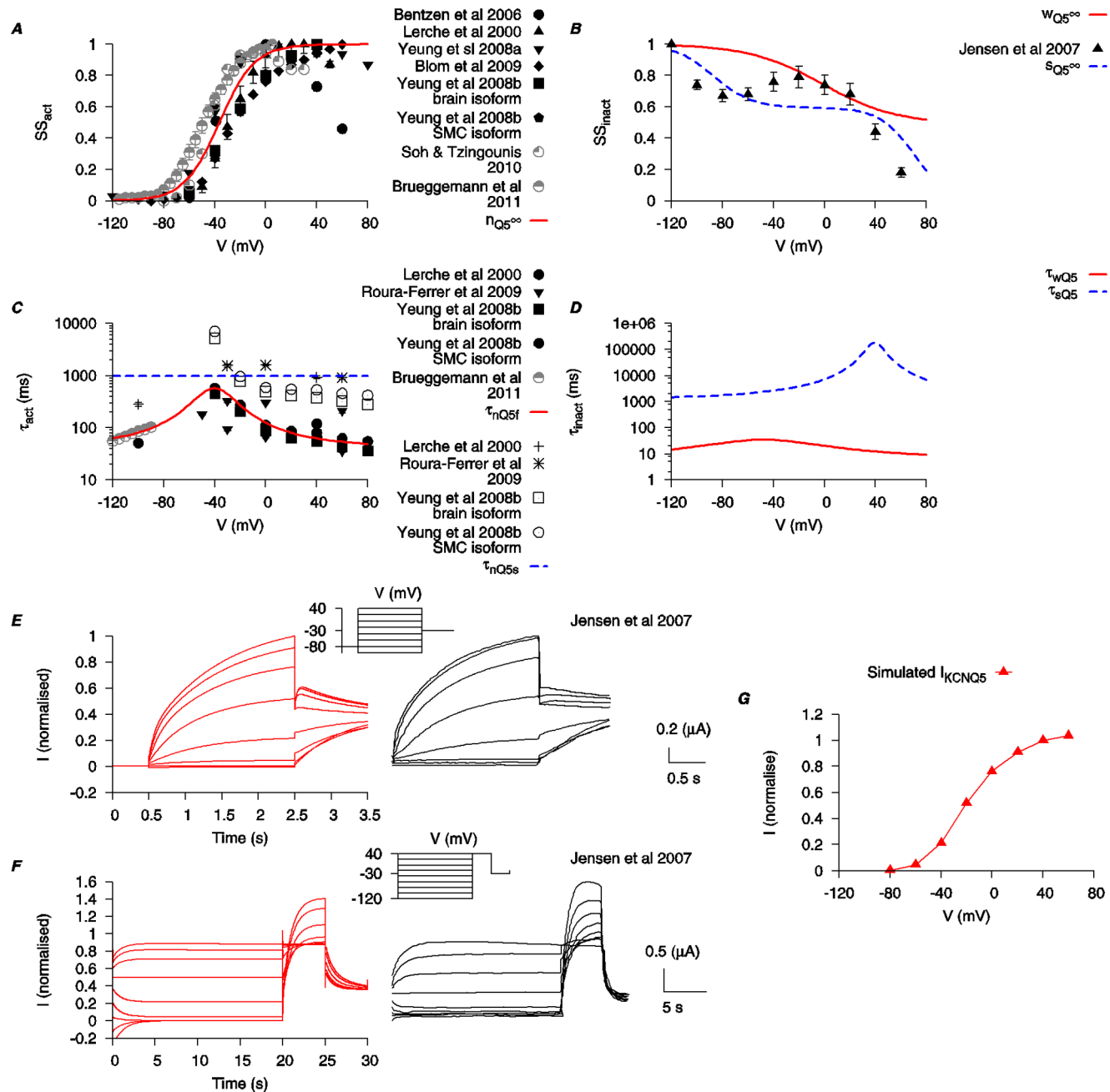


Figure 5. Biophysical characteristics of KCNQ5 current. Properties of I_{KCNQ5} are developed using experimental data from cloned mammalian KCNQ5 expressed in *Xenopus laevis* oocytes (black) and other expression systems (gray) [31, 32, 34, 36, 38–42]. A, V-dependent activation steady state (n_{Q5}^{∞}). B, V-dependent steady states for fast inactivation (w_{Q5}^{∞}) and slow inactivation (s_{Q5}^{∞}). C, V-dependent activation time constants (τ_{nQ5f} and τ_{nQ5s}). τ_{nQ5f} is V-dependent but τ_{nQ5s} is set as a constant at 1 s. D, V-dependent time constants for fast inactivation (τ_{wQ5}) and slow inactivation (τ_{sQ5}). E and F, simulated time tracings of I_{KCNQ5} with two different voltage-clamp protocols (insets) used in Jensen et al. (2007) [32] and the experimental time tracings are shown for comparison. (Experimental tracing adapted with permission from Jensen et al. (2007); copyright 2007, Biophysical Society.) G, simulated I - V relationship of I_{KCNQ5} using the same voltage-clamp protocol as in E. All I - V data are normalized to the maximal current value at $V=40$ mV.

doi:10.1371/journal.pone.0114034.g005

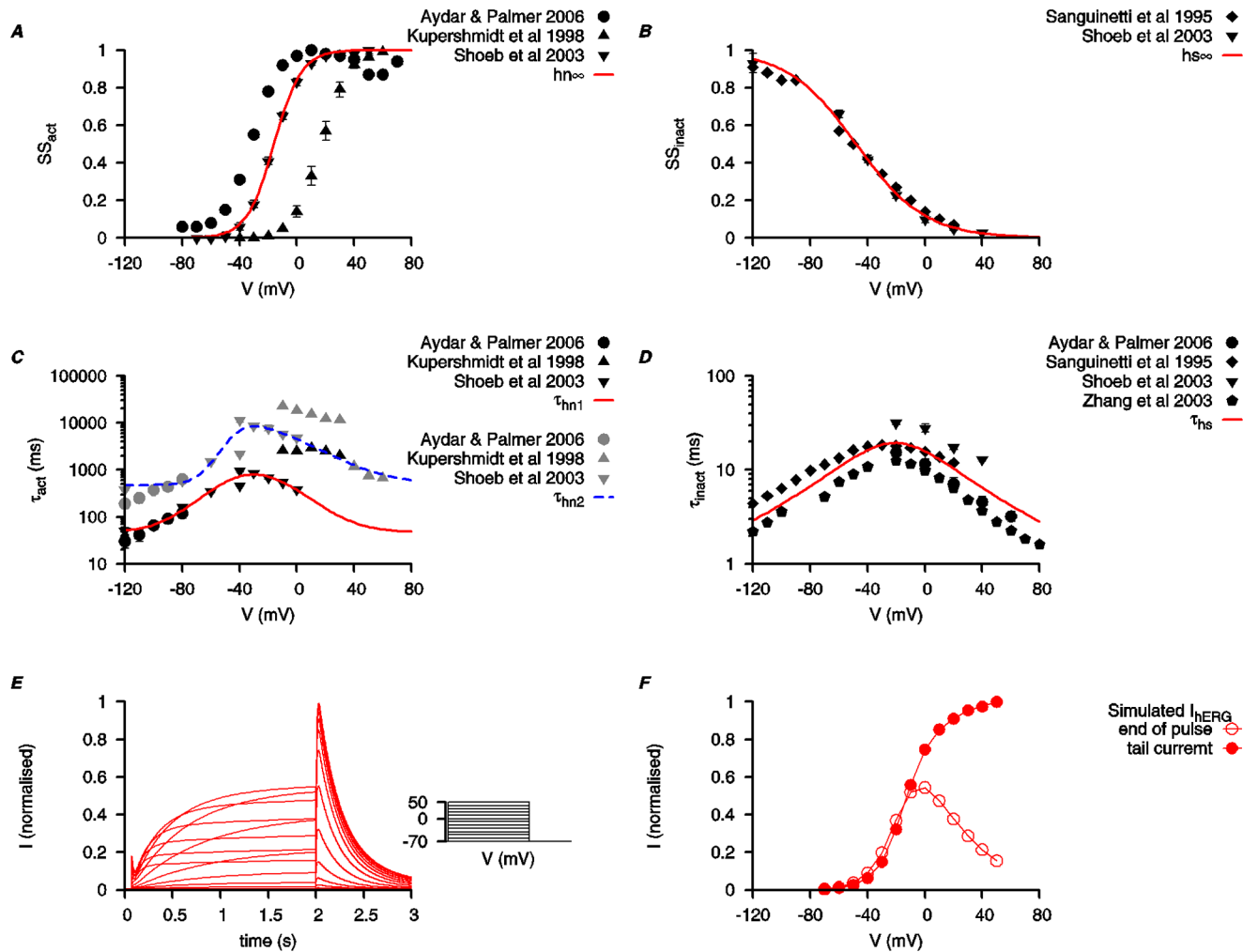


Figure 6. Biophysical characteristics of hERG current. Properties of I_{hERG} for the myometrial cell model are developed using experimental data from full length hERG clones expressed in different expression systems [15, 16, 19, 20, 43]. A, V-dependent activation steady state (h_{∞}). B, V-dependent inactivation steady state ($h_{s\infty}$). C, V-dependent activation time constants (τ_{hn1} and τ_{hn2}). D, V-dependent inactivation time constant (τ_{hs}). E, simulated time tracings of I_{hERG} . Currents were evoked from a holding potential (V_h) of -70 mV to various voltage steps (V_{step}) for 2 s then stepped back to V_h . F, simulated $I-V$ relationships of I_{hERG} using the same voltage-clamp protocol as in E. Both the currents at the end of V_{step} (empty points) and the following maximal tail currents after the end of V_{step} (solid points) were plotted against V_{step} . In both E and F, all data are normalized to the peak tail current value at $V=60$ mV.

doi:10.1371/journal.pone.0114034.g006

Substitution of I_{K1} in the USMC model by individual KCNQ or hERG currents

As rationalized above, in points (i)–(vii), I_{KCNQ} or I_{hERG} or both could be constituent components of the global, rather ill-defined uterine K^+ current measured as I_{K1} . We proceeded, therefore, to assess if I_{K1} in the USMC model could be replaced by I_{KCNQ} or I_{hERG} or a combination of each. As there is little information about the current densities for I_{KCNQ} or I_{hERG} in uterine cells, and the expression of uterine KCNQ and hERG subunits changes during pregnancy, we fitted the values of their maximal conductances so that the simulated maximal

whole cell K^+ currents matched the experimental value from Wang et al. (1998) [44].

First, we attempted to completely replace I_{K1} in the USMC model with, in turn, I_{KCNQ1} , I_{KCNQ4} , I_{KCNQ5} or I_{hERG} . In particular, we were interested in seeing if this could change the AP forms. Each of these maneuvers resulted in the simulation of interesting long-duration AP forms, including a long bursting-type AP form (Figure S1). However, in each case, the corresponding simulations of whole cell K^+ current tracings and I-V plots did not match the experimental data (middle and right panels of Figure S1B-E). In native USMC cells [5, 44], and in the original USMC model [4], the majority of myometrial I_{K1} would be inactivated by a holding potential (V_h) of -40 mV due to the negative half inactivation of I_{K1} . So, under voltage-clamped conditions, a larger outward K^+ current would be evoked from a V_h of -80 mV compared to the current evoked from a V_h of -40 mV (Figure S1A middle panel). However, with complete replacement of I_{K1} by individual I_{KCNQ1} , I_{KCNQ4} , I_{KCNQ5} or I_{hERG} , the resultant whole cell steady-state K^+ current amplitude was the same when evoked from either V_h . This was a deviation from the previously matched experimental results. Nonetheless, this exercise showed that I_{KCNQ} or I_{hERG} , could contribute to the development of long duration burstings APs in uterine cells.

Next, we partially replaced I_{K1} in the cell model with, in turn, I_{KCNQ1} , I_{KCNQ4} , I_{KCNQ5} or I_{hERG} , while ensuring the simulated whole cell K^+ current matched to the experimental data from Wang et al. (1998) [44]. With the standard model configuration, before any changes were implemented, $\bar{g}_{K1} = 0.52$ nS pF^{-1} (Figure S2A). We proceeded with the partial substitution in steps. The level of I_{K1} was first reduced by changing \bar{g}_{K1} to 0.24 nS pF^{-1} (Figure S2B). At this reduced level of I_{K1} , the long-duration AP configuration shows only a plateau-type form with no initial bursting. However, the voltage-clamp experimental results for the whole cell K^+ current from different holding potentials can still be reproduced and so this level of I_{K1} was chosen as a reasonable modification with which to investigate the effects of partially replacing I_{K1} by I_{KCNQ} or I_{hERG} . Within the constrain of matching the experimental whole cell K^+ currents (middle panels) and the I-V relationships (right panels) from Wang et al. (1998) [44], we identified the conductance ranges for I_{KCNQ} or I_{hERG} that favor long-duration bursting APs. With reduced I_{K1} and incremental additions of I_{KCNQ1} , within a \bar{g}_{KCNQ1} range of $0.026 - 0.042$ nS pF^{-1} , complex AP forms could be simulated whereby the AP plateau was interspersed with periodic bursting (Figure S2B-E). Alternatively, with reduced I_{K1} and incremental additions of I_{KCNQ4} , within a \bar{g}_{KCNQ4} range of $0.03216 - 0.04712$ nS pF^{-1} there was an increasing tendency towards bursting behavior persisting throughout the AP albeit with diminishing amplitude (Figure S3C-E). With reduced I_{K1} and incremental additions of I_{hERG} , within a \bar{g}_{hERG} range of $0.112 - 0.208$ nS pF^{-1} , there was an increasing tendency towards improving the bursting behavior of long-duration AP (Figure S5C-E). In contrast, if the reduced I_{K1} was replaced with incremental additions of I_{KCNQ5} , there was no observable change in the AP form from that of a plateau-type AP (Figure S4C-E, left panel).

The tendency of I_{KCNQ1} , I_{KCNQ4} or I_{hERG} , to improve the bursting potential of the AP form, suggested that each current individually - I_{KCNQ1} , I_{KCNQ4} or I_{hERG} - could improve the capabilities of the USMC model in the manner we set out to achieve. For I_{KCNQ5} the situation appeared different to the other three currents in that after its partial replacement of I_{K1} the AP forms remained tonic and plateau-like (Figure S4). The effect of incremental inclusion of I_{KCNQ5} was to reduce the plateau potential and the resting membrane potential. Thus I_{KCNQ5} does not seem to play a role in bursting APs generation. In addition, there may be species-dependent differences in KCNQ5 expression patterns close to term and/or during labor with human myometrium expressing less KCNQ5 than KCNQ1 or KCNQ4 [8]. This, coupled to the rather negative membrane potentials for activation of the current (Figure 5A), led us to speculate that if I_{KCNQ5} is to have a role in USMC, it may be for setting the level of resting membrane potential or plateau potential or both rather than contributing to the macroscopic action potential generated K^+ current. In our formulation of the original USMC model [4], a background K^+ current, I_b , was included to represent a collection of minor K^+ currents with unknown kinetics that were necessary to hold the membrane potential at physiologically relevant resting levels. The above information suggested that the biophysically detailed I_{KCNQ5} may ably replace the rather vaguely defined I_b . Indeed, when this was done, the cell model was still capable of reproducing all the previous validation results (data not shown). Moreover, with a small increase in I_{KCNQ5} , the model repolarized at the end of the stimulation, while in the original cell model, a small increase of I_b did not cause the same behavior (data not shown). Furthermore, replacing I_b with I_{KCNQ5} did not affect the results of partially substituting I_{K1} by I_{KCNQ1} , I_{KCNQ4} or I_{hERG} (data not shown). Thus, our first confirmed modification of the initial USMC cell model [4] was to replace I_b with I_{KCNQ5} .

Given that uterine smooth muscle cells express components of KCNQ and hERG channels in a gestational dependent manner, we sought to test the proposition that the long duration bursting APs would be facilitated by the incorporation of a combination of I_{KCNQ1} , I_{KCNQ4} and I_{hERG} in place of reduced I_{K1} (Figure 7A). Implementation of this scenario - with reduced I_{K1} ($\bar{g}_{K1} = 0.24$ nS pF^{-1}), a combination of I_{KCNQ1} ($\bar{g}_{KCNQ1} = 0.0032$ nS pF^{-1}), I_{KCNQ4} ($\bar{g}_{KCNQ4} = 0.024$ nS pF^{-1}) and I_{hERG} ($\bar{g}_{hERG} = 0.08$ nS pF^{-1}) and with I_b replaced by I_{KCNQ5} ($\bar{g}_{KCNQ5} = 0.016$ nS pF^{-1}) - accomplished our objective of reproducing the experimentally reported long-duration bursting AP forms [1–3]. Thus by incorporating biophysical details of I_{KCNQ1} , I_{KCNQ4} , I_{KCNQ5} and I_{hERG} , these modifications corrected a main limitation of the original USMC model. It is likely that this was accomplished by strengthening the repolarization reserve [45] of the uterine cell thereby providing more ways to shape the USMC APs.

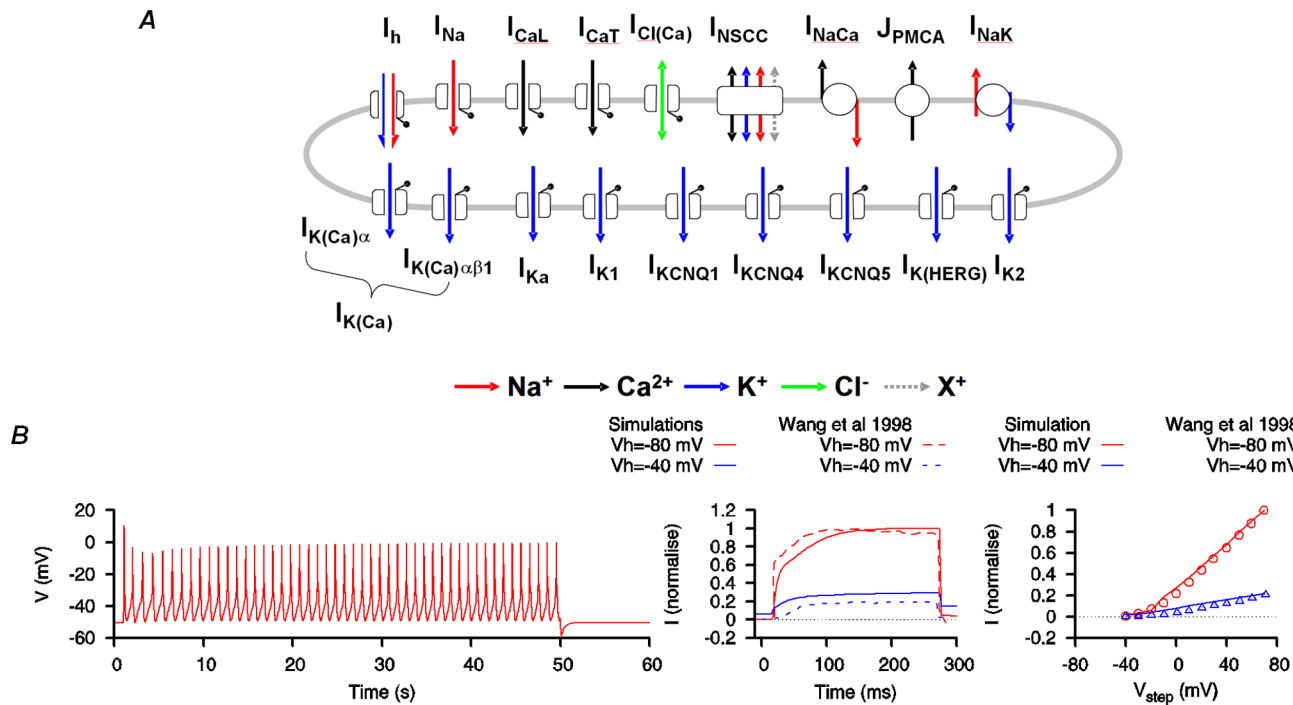


Figure 7. USMC model modification with incorporation of KCNQ1, KCNQ4, KCNQ5 and hERG currents. A, Effect of I_{K1} being partially replaced by a combination of I_{KCNQ1} ($\bar{g}_{KCNQ1} = 0.0032 \text{ nS pF}^{-1}$), I_{KCNQ4} ($\bar{g}_{KCNQ4} = 0.024 \text{ nS pF}^{-1}$) and I_{hERG} ($\bar{g}_{hERG} = 0.08 \text{ nS pF}^{-1}$). Note that I_b has been replaced with I_{KCNQ5} ($\bar{g}_{KCNQ5} = 0.016 \text{ nS pF}^{-1}$). With this configuration, long-duration bursting APs were induced (left panel) while the whole cell K^+ currents (middle panel) and the I - V relationships (right panel) matched the experimental data [44] (© Wang et al., 1998). B, Summary of the electrogenic components of the modified USMC model.

doi:10.1371/journal.pone.0114034.g007

Effects of changing hERG current conductance on USMC action potentials

Each of I_{KCNQ1} , I_{KCNQ4} or I_{hERG} contributed to the ability of the *modified USMC* model to produce longer bursting APs. Of these, I_{hERG} appeared to exert the most potent influence in this regard (Figure S5). Indeed, in other electrically excitable cells, I_{hERG} contributes to AP spike frequency adaptation [46]. It is noteworthy that hERG-like currents have been reported to be decreased in murine and human myometrial tissues at late pregnancy [13, 14]. Our simulations also showed that progressive reductions in I_{hERG} conductance changed the simulated AP form from that of the long duration bursting AP (Figure 8A) to a more tonic plateau-type AP (Figure 8B-E). This result is similar to the effect of dofetilide on human myometrial APs [14] and provides a validation for the *modified USMC* model.

Potential effects of changing both KCNQ and hERG current conductances on USMC action potentials

Both KCNQ and hERG currents are present in cardiac muscles and each contributes to stable and timely repolarization [45]. In uterine tissues, the regulations of KCNQ and hERG currents, and/or their molecular components,

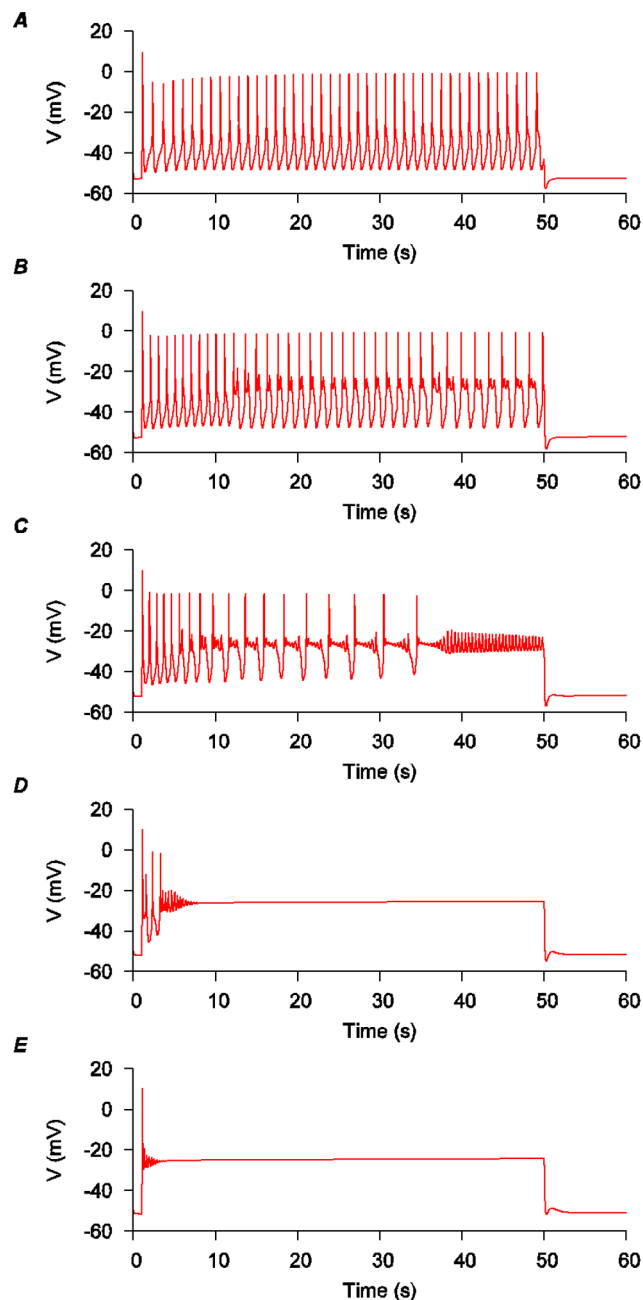


Figure 8. Effects of changing hERG current conductance on the modified USMC model AP form. A, The same conditions and AP form of the modified USMC model as depicted in Figure 7 wherein $\bar{g}_{\text{hERG}} = 0.08 \text{ nS pF}^{-1}$. B-E, the effects of progressively reducing I_{hERG} conductance. B, $\bar{g}_{\text{hERG}} = 0.0464 \text{ nS pF}^{-1}$; C, $\bar{g}_{\text{hERG}} = 0.0224 \text{ nS pF}^{-1}$; D, $\bar{g}_{\text{hERG}} = 0.0064 \text{ nS pF}^{-1}$; E, $\bar{g}_{\text{hERG}} = 0.0008 \text{ nS pF}^{-1}$.

doi:10.1371/journal.pone.0114034.g008

appear different from each other. Currents sensitive to hERG inhibitors have been reported in uterine tissues in early to mid gestation but these are decreased close to term [13, 14]. In contrast, almost all KCNQ alpha subunits expressions were suppressed during early to mid-gestation and increased at late term [8]. These

data suggest KCNQ and hERG currents/components are gestationally regulated in a different manner and raises the question what may the effect be of changing the contributions of each of these particular K^+ channel conductances? We utilized simulations of the *modified USMC* model to examine this.

We began our simulations with no KCNQ currents but with full hERG current (Figure 9A). The result was a plateau-type AP with no initial bursting, qualitatively similar to the plateau-type APs recorded from uterine smooth muscle cells of mid-gestation pregnant rats [1]. We then examined the effects of either increasing I_{KCNQ} or reducing I_{hERG} . With a little I_{KCNQ} , but no change in I_{hERG} , complex oscillations of membrane potentials began to develop around the plateau level (Figure 9B). With more I_{KCNQ} , but still no change in I_{hERG} , a bursting-type AP could be formed (Figure 9C), qualitatively similar to those bursting-type APs recorded from the uterine smooth muscle cells at end-of-term in rats [1]. Note that this is the configuration for our *modified USMC* model described in previous sections. Further increase of I_{KCNQ} , and still no change in I_{hERG} , suppressed the AP (Figure 9D). (As we do not know the maximum quantities of I_{KCNQ} in uterine smooth muscle cells, it is entirely possible for the I_{KCNQ} to exceed our reference (1.0) values). With I_{KCNQ} staying at the same level, but with reduced I_{hERG} , the bursting-type AP can be formed again (Figure 9E). Further reduction of I_{hERG} suppressed the size of the bursting spikes and changed the AP into a complex form (Figure 9F). These simulations show that although I_{KCNQ} and I_{hERG} may be inversely regulated at late pregnancy, the alteration of conductances for each current potentially yields a fine tuning mechanism for uterine cells to develop and maintain long-duration bursting AP forms that are required for parturition.

Conclusions and future considerations

We have identified I_{KCNQ} and I_{hERG} as important components for forming the characteristic long duration bursting-type APs of uterine smooth muscle cells. Also, the above computational approaches have enabled the establishment of a biophysically detailed mathematical model of uterine smooth muscle cell electrical excitability that reproduces the repertoire of experimentally-derived AP forms. In addition, this computational work alerts one to important biological features that would otherwise not be foreseen and can serve as an important tool for hypotheses generations and subsequent experimental testing. A key example is the model prediction that alterations of I_{KCNQ} and I_{hERG} have the potential to radically affect uterine AP forms and, as such, suggests that the physiological regulations of I_{KCNQ} and I_{hERG} may be crucial factors in determining labor onset and maintenance. Of note, there is increasing appreciation of the important roles that computational biology can make to improving our understanding of the complexities of uterine excitability and labor onset [47–48], to which the open-access *modified USMC* model herein looks to contribute by providing the research community with the opportunity to iteratively improve upon the biophysical detail of the components. This will include considerations of intracellular (e.g. metabolic-excitation-contraction coupling characteristics [49] and Ca^{2+} binding protein affinities) and intercellular (e.g. interstitial K^+

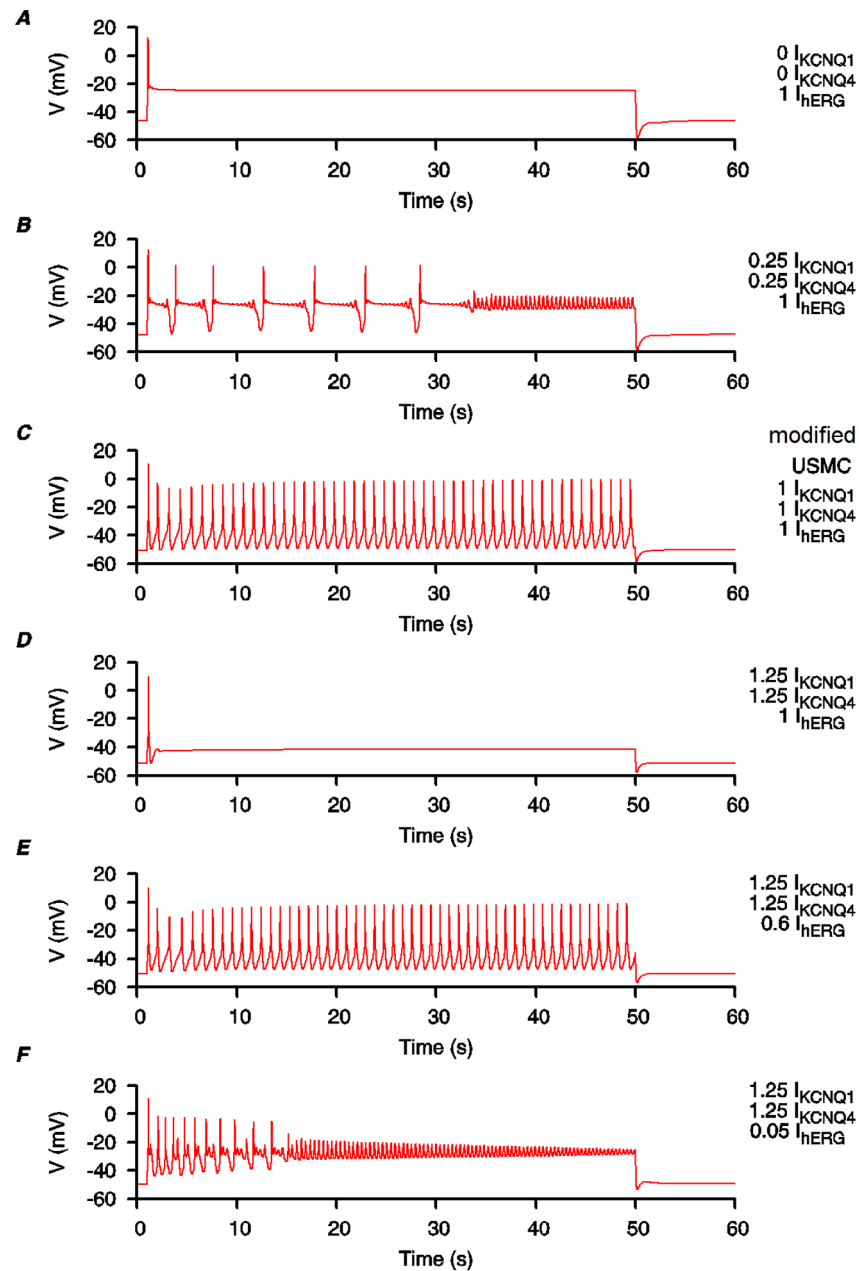


Figure 9. Effects of changing KCNQ and hERG current conductances on the *modified USMC* model AP form. Simulating the effects of increased expression of KCNQ subunits and reduction of HERG current in uterine smooth muscle cells during late term. The conductance values for I_{KCNQ} and I_{hERG} in the *modified USMC* model, as in Figure 7, are used as the reference values. Both I_{KCNQ1} and I_{KCNQ4} were changed by the same proportions. A, no I_{KCNQ1} or I_{KCNQ4} ; I_{hERG} at 1 fold. B, I_{KCNQ1} and I_{KCNQ4} at 0.25 fold; I_{hERG} at 1 fold. C, I_{KCNQ1} , I_{KCNQ4} and I_{hERG} at 1 fold. D, I_{KCNQ1} and I_{KCNQ4} at 1.25 fold; I_{hERG} at 1 fold. E, I_{KCNQ1} and I_{KCNQ4} at 1.25 fold; I_{hERG} at 0.6 fold. F, I_{KCNQ1} and I_{KCNQ4} at 1.25 fold; I_{hERG} at 0.05 fold.

doi:10.1371/journal.pone.0114034.g009

accumulation [50]) mechanisms that may act on ionic currents to modulate AP form. To provide tissue-level models that encapsulate the whole process of excitation-contraction coupling one also has to consider spatio-temporal patterns of excitation

[48]. Notwithstanding these longer-term research aspirations, our modified model of uterine cell excitability adds to our wider knowledge of the molecular and electrophysiological basis of cellular rhythms [51].

Methods

The original USMC model from [4] describing 14 electrogenic membrane currents, intracellular calcium changes and associated force was used as the basis of this study. Detailed descriptions of the model equations and parameters values are given in [4].

This theoretical study was conducted in two parts. First, we performed an extensive one-at-a-time sensitivity analysis [52] on the USMC model kinetic properties to identify potential target parameters that can prolong or improve the initial bursting in an AP. Then, based on the results, we focused on including more kinetic details of the delay rectifying K^+ currents. The USMC model is then modified by including four new voltage-gated K^+ currents from the KCNQ and HERG families: I_{KCNQ1} , I_{KCNQ4} , I_{KCNQ5} and I_{HERG} . The kinetics of these four K^+ currents were described by Hodgkin-Huxley type formulations using published clonal data in various expression systems as there are no published data from myometrial cells or tissues. The details of these currents are described in the Results and Discussion. The definitions of the symbols, the initial conditions and parameters values, the equations of the new potassium currents and the resulting *modified USMC* model are given in Table S1–3 and Appendix S1. The source code of the *modified USMC* model written in the C programming language is included in Appendix S2.

Unless otherwise stated, all simulated APs were evoked with a 50 s current clamp stimulus of -0.25 pA pF^{-1} at $t=1 \text{ s}$ starting from the same initial conditions. For each maneuver of incorporating new currents into the cell model, the whole cell K^+ currents and the corresponding I - V relationships were also constructed and validated against existing experimental data. Both the whole cell K^+ currents and the I - V relationships were simulated by the same one-step voltage-clamp protocol: the membrane voltage was stepped up from a holding potential (V_h) of either -40 mV or -80 mV to a step potential (V_{step}) between -40 mV to 70 mV for 250 ms before stepping back to the V_h . The model was started at the steady state conditions at V_h for each voltage-clamp step. For clarity, and to aid the readers comparison with the corresponding experimental time tracings from Wang et al. (1998) [44], only one simulated time tracing at $V_{\text{step}} = 0 \text{ mV}$ from each of the two V_h conditions were shown in our figures and Supplementary figures, and both the simulated and the extracted experimental time tracings were normalized to the maximal value from $V_h = -80 \text{ mV}$. The simulated I - V relationships were constructed from the maximum currents at each of the V_{step} normalized to the peak value at $V_{\text{step}} = 70 \text{ mV}$ from $V_h = -80 \text{ mV}$.

Simulations were computed with a fixed time step of 0.02 ms , using XPPAUT [53] with the fourth-order Runge-Kutta numerical integration method, in a IBM laptop PC with a Intel(R) Pentium(R) M 1.5 GHz single processor.

Supporting Information

Figure S1. I_{K1} cannot be completely replaced by KCNQ1, KCNQ4, KCNQ5 or hERG current. Effects of I_{K1} being completely replaced by either I_{KCNQ1} , I_{KCNQ4} , I_{KCNQ5} or I_{hERG} . A, left hand panel: the standard configuration of the initial USMC model ($\bar{g}_{K1} = 0.52 \text{ nS pF}^{-1}$), as depicted in [Figure 1C](#), before I_{K1} replacement; middle panel: two simulated USMC whole cell K^+ currents (*solid lines*) at a V_h step of 0 mV, one tracing was from a V_h of -40 mV (*blue*) and another from a V_h of -80 mV (*red*), and the corresponding experimental time tracings (*broken lines*) of Wang et al. (1998) [44] (© Wang et al., 1998); right hand panel: the simulated USMC K^+ I - V relationships (*lines*) from both V_h and the corresponding experimental data (*points*) of Wang et al., (1998) [44] (© Wang et al., 1998). B-E, the effects of I_{K1} being replaced by: B, I_{KCNQ1} , C, I_{KCNQ4} , D, I_{KCNQ5} and E, I_{hERG} .
[doi:10.1371/journal.pone.0114034.s001](https://doi.org/10.1371/journal.pone.0114034.s001) (TIF)

Figure S2. USMC model modification with reduced I_{K1} and added KCNQ1 current. Effects of I_{K1} being partially replaced by I_{KCNQ1} . A, the standard model configuration ($\bar{g}_{K1} = 0.52 \text{ nS pF}^{-1}$) before I_{K1} replacement. Left hand panel: the standard AP simulation as depicted in [Figure 1C](#); middle panel and right hand panel: the whole cell USMC I - V data. B-E, reduced I_{K1} ($\bar{g}_{K1} = 0.24 \text{ nS pF}^{-1}$) with different levels of KCNQ1 added: B, $\bar{g}_{KCNQ1} = 0 \text{ nS pF}^{-1}$; C, $\bar{g}_{KCNQ1} = 0.028 \text{ nS pF}^{-1}$; D, $\bar{g}_{KCNQ1} = 0.032 \text{ nS pF}^{-1}$; E, $\bar{g}_{KCNQ1} = 0.036 \text{ nS pF}^{-1}$.
[doi:10.1371/journal.pone.0114034.s002](https://doi.org/10.1371/journal.pone.0114034.s002) (TIF)

Figure S3. USMC model modification with reduced I_{K1} and added KCNQ4 current. Effects of I_{K1} being partially replaced by I_{KCNQ4} . A, the standard model configuration ($\bar{g}_{K1} = 0.52 \text{ nS pF}^{-1}$) before I_{K1} replacement. Left hand panel: the standard AP simulation as depicted in [Figure 1C](#); middle panel and right hand panel: the whole cell USMC I - V data. B-E, reduced I_{K1} ($\bar{g}_{K1} = 0.24 \text{ nS pF}^{-1}$) with different levels of KCNQ4 added: B, $\bar{g}_{KCNQ4} = 0 \text{ nS pF}^{-1}$; C, $\bar{g}_{KCNQ4} = 0.03568 \text{ nS pF}^{-1}$; D, $\bar{g}_{KCNQ4} = 0.0392 \text{ nS pF}^{-1}$; E, $\bar{g}_{KCNQ4} = 0.04272 \text{ nS pF}^{-1}$.
[doi:10.1371/journal.pone.0114034.s003](https://doi.org/10.1371/journal.pone.0114034.s003) (TIF)

Figure S4. USMC model modification with reduced I_{K1} and added KCNQ5 current. Effects of I_{K1} being partially replaced by I_{KCNQ5} . A, the standard model configuration ($\bar{g}_{K1} = 0.52 \text{ nS pF}^{-1}$) before I_{K1} replacement. Left hand panel: the standard AP simulation as depicted in [Figure 1C](#); middle panel and right hand panel: the whole cell USMC I - V data. B-E, reduced I_{K1} ($\bar{g}_{K1} = 0.24 \text{ nS pF}^{-1}$) with different levels of KCNQ5 added: B, $\bar{g}_{KCNQ5} = 0 \text{ nS pF}^{-1}$; C, $\bar{g}_{KCNQ5} = 0.0192 \text{ nS pF}^{-1}$; D, $\bar{g}_{KCNQ5} = 0.02 \text{ nS pF}^{-1}$; E, $\bar{g}_{KCNQ5} = 0.0208 \text{ nS pF}^{-1}$.
[doi:10.1371/journal.pone.0114034.s004](https://doi.org/10.1371/journal.pone.0114034.s004) (TIF)

Figure S5. USMC model modification with reduced I_{K1} and added hERG current. Effects of I_{K1} being partially replaced by I_{hERG} . A, the standard model configuration ($\bar{g}_{K1} = 0.52 \text{ nS pF}^{-1}$) before I_{K1} replacement. Left hand panel: the standard AP simulation as depicted in [Figure 1C](#); middle panel and right hand panel: the whole cell USMC I - V data. B-E, reduced I_{K1} ($\bar{g}_{K1} = 0.24 \text{ nS pF}^{-1}$) with

different levels of hERG added: *B*, $\bar{g}_{\text{hERG}}=0$ nS pF⁻¹; *C*, $\bar{g}_{\text{hERG}}=0.112$ nS pF⁻¹; *D*, $\bar{g}_{\text{hERG}}=0.144$ nS pF⁻¹; *E*, $\bar{g}_{\text{hERG}}=0.176$ nS pF⁻¹.

[doi:10.1371/journal.pone.0114034.s005](https://doi.org/10.1371/journal.pone.0114034.s005) (TIF)

Table S1. Definitions of the equation symbols.

[doi:10.1371/journal.pone.0114034.s006](https://doi.org/10.1371/journal.pone.0114034.s006) (PDF)

Table S2. Initial values of the dynamical variables used for the *modified USMC* model.

[doi:10.1371/journal.pone.0114034.s007](https://doi.org/10.1371/journal.pone.0114034.s007) (PDF)

Table S3. Constant parameter values used for the *modified USMC* model.

[doi:10.1371/journal.pone.0114034.s008](https://doi.org/10.1371/journal.pone.0114034.s008) (PDF)

Appendix S1. Equations used for the *modified USMC* model.

[doi:10.1371/journal.pone.0114034.s009](https://doi.org/10.1371/journal.pone.0114034.s009) (PDF)

Appendix S2. Source codes in C for the *modified USMC* model.

[doi:10.1371/journal.pone.0114034.s0010](https://doi.org/10.1371/journal.pone.0114034.s0010) (BZ2)

Author Contributions

Conceived and designed the experiments: MJT WCT. Performed the experiments: WCT. Analyzed the data: MJT WCT. Wrote the paper: MJT WCT RMT RS.

References

1. **Wilde DW, Marshall JM** (1988) Effects of tetraethylammonium and 4-aminopyridine on the plateau potential of circular myometrium from the pregnant rat. *Biol Reprod* 38: 836–845.
2. **Inoue Y, Okabe K, Soeda H** (1999) Augmentation and suppression of action potentials by estradiol in the myometrium of pregnant rat. *Can J Physiol Pharmacol* 77: 447–453.
3. **Khan RN, Smith SK, Morrison JJ, Ashford ML** (1997) Ca²⁺ dependence and pharmacology of large-conductance K⁺ channels in nonlabor and labor human uterine myocytes. *Am J Physiol* 273: C1721–C1731.
4. **Tong WC, Choi CY, Kharche S, Holden AV, Zhang H, et al.** (2011) A computational model of the ionic currents, Ca²⁺ dynamics and action potentials underlying contraction of isolated uterine smooth muscle. *PLoS ONE* 6: e18685.
5. **Knock GA, Smirnov SV, Aaronson PI** (1999) Voltage-gated K⁺ currents in freshly isolated myocytes of the pregnant human myometrium. *J Physiol* 518: 769–781.
6. **Boyle MB, MacLusky NJ, Naftolin F, Kaczmarek LK** (1987) Hormonal regulation of K⁺-channel messenger RNA in rat myometrium during oestrus cycle and in pregnancy. *Nature* 330: 373–375.
7. **Boyle MB, Azhderian EM, MacLusky NJ, Naftolin F, Kaczmarek LK** (1987) *Xenopus oocytes* injected with rat uterine RNA express very slowly activating potassium currents. *Science* 235: 1221–1224.
8. **McCallum LA, Pierce SL, England SK, Greenwood IA, Tribe RM** (2011) The contribution of Kv7 channels to pregnant mouse and human myometrial contractility. *J Cell Mol Med* 15: 577–586.
9. **Bendahhou S, Marionneau C, Haurogne K, Larroque MM, Derand R, et al.** (2005) *In vitro* molecular interactions and distribution of KCNE family with KCNQ1 in the human heart. *Cardiovasc Res* 67: 529–538.
10. **Yeung SYM, Greenwood IA** (2005) Electrophysiological and functional effects of the KCNQ channel blocker XE991 on murine portal vein smooth muscle cells. *Br J Pharmacol* 146: 585–595.

11. **Hadley JK, Noda M, Selyanko AA, Wood IC, Abogadie FC, et al.** (2000) Differential tetraethylammonium sensitivity of KCNQ1-4 potassium channels. *Br J Pharmacol* 129: 413–415.
12. **Robbins J** (2001) KCNQ potassium channels: physiology, pathophysiology, and pharmacology. *Pharmacol Ther* 90: 1–19.
13. **Greenwood IA, Yeung SY, Tribe RM, Ohya S** (2009) Loss of functional K⁺ channels encoded by ether-à-go-go-related genes in mouse myometrium prior to labour onset. *J Physiol* 587: 2313–2326.
14. **Parkington HC, Stevenson J, Tonta MA, Paul J, Butler T, et al.** (2014) Diminished hERG K⁺ channel activity facilitates strong human labour contractions but is dysregulated in obese women. *Nat Commun* 17;5:4108.
15. **Sanguinetti MC, Jiang C, Curran ME, Keating MT** (1995) A mechanistic link between an inherited and an acquired cardiac arrhythmia: HERG encodes the IKr potassium channel. *Cell* 81: 299–307.
16. **Shoeb F, Malykhina AP, Akbarali HI** (2003) Cloning and functional characterization of the smooth muscle ether-à-go-go-related gene K⁺ channel. potential role of a conserved amino acid substitution in the S4 region. *J Biol Chem* 278: 2503–2514.
17. **Larsen AP, Olesen SP, Grunnet M, Jespersen T** (2008) Characterization of hERG1a and hERG1b potassium channels—a possible role for hERG1b in the I(Kr) current. *Pflugers Arch* 456(6):1137–48.
18. **Wang S, Morales MJ, Liu S, Strauss HC, Rasmusson RL** (1996) Time, voltage and ionic concentration dependence of rectification of h-erg expressed in *Xenopus oocytes*. *FEBS Lett* 389(2):167–73.
19. **Aydar E, Palmer C** (2006) Expression and functional characterization of the human ether-à-go-go-related gene (HERG) K⁺ channel cardiac splice variant in *Xenopus laevis* oocytes. *J Membr Biol* 211: 115–126.
20. **Kupersmidt S, Snyders DJ, Raes A, Roden DM** (1998) A K⁺ channel splice variant common in human heart lacks a C-terminal domain required for expression of rapidly activating delayed rectifier current. *J Biol Chem* 273: 27231–27235.
21. **Yeung SY, Greenwood IA** (2007) Pharmacological and biophysical isolation of K⁺ currents encoded by ether-à-go-go-related genes in murine hepatic portal vein smooth muscle cells. *Am J Physiol Cell Physiol* 292(1):C468–76.
22. **London B, Trudeau MC, Newton KP, Beyer AK, Copeland NG, et al.** (1997) Two isoforms of the mouse ether-à-go-go-related gene coassemble to form channels with properties similar to the rapidly activating component of the cardiac delayed rectifier K⁺ current. *Circ Res* 81: 870–878.
23. **Tristani-Firouzi M, Sanguinetti MC** (1998) Voltage-dependent inactivation of the human K⁺ channel KvLQT1 is eliminated by association with minimal K⁺ channel (minK) subunits. *J Physiol* 510(1): 37–45.
24. **Franqueza L, Lin M, Shen J, Splawski I, Keating MT, et al.** (1999) Long QT syndrome-associated mutations in the S4-S5 linker of KvLQT1 potassium channels modify gating and interaction with minK subunits. *J Biol Chem* 274: 21063–21070.
25. **Selyanko AA, Hadley JK, Wood IC, Abogadie FC, Jentsch TJ, et al.** (2000) Inhibition of KCNQ1-4 potassium channels expressed in mammalian cells via M1 muscarinic acetylcholine receptors. *J Physiol* 522(3):349–355.
26. **Pusch M, Ferrera L, Friedrich T** (2001) Two open states and rate-limiting gating steps revealed by intracellular Na⁺ block of human KCNQ1 and KCNQ1/KCNE1 K⁺ channels. *J Physiol* 533: 135–143.
27. **Seebohm G, Lerche C, Pusch M, Steinmeyer K, Brggemann A, et al.** (2001) A kinetic study on the stereospecific inhibition of KCNQ1 and I(Ks) by the chromanol 293B. *Br J Pharmacol* 134: 1647–1654.
28. **Peretz A, Schottelndreier H, Aharon-Shamgar LB, Attali B** (2002) Modulation of homomeric and heteromeric KCNQ1 channels by external acidification. *J Physiol* 545: 751–766.
29. **Gibor G, Yakubovich D, Peretz A, Attali B** (2004) External barium affects the gating of KCNQ1 potassium channels and produces a pore block via two discrete sites. *J Gen Physiol* 124: 83–102.
30. **Seebohm G, Strutz-Seebohm N, Baltaev R, Korniychuk G, Knirsch M, et al.** (2005) Regulation of KCNQ4 potassium channel prepulse dependence and current amplitude by SGK1 in *Xenopus oocytes*. *Cell Physiol Biochem* 16: 255–262.
31. **Bentzen BH, Schmitt N, Calloe K, Brown WD, Grunnet M, et al.** (2006) The acrylamide (S)-1 differentially affects Kv7 (KCNQ) potassium channels. *Neuropharmacology* 51: 1068–1077.

32. **Jensen HS, Grunnet M, Olesen SP** (2007) Inactivation as a new regulatory mechanism for neuronal Kv7 channels. *Biophys J* 92: 2747–2756.
33. **Gao Z, Xiong Q, Sun H, Li M** (2008) Desensitization of chemical activation by auxiliary subunits: convergence of molecular determinants critical for augmenting KCNQ1 potassium channels. *J Biol Chem* 283: 22649–22658.
34. **Blom SM, Schmitt N, Jensen HS** (2009) The acrylamide (S)-2 as a positive and negative modulator of Kv7 channels expressed in *Xenopus laevis* oocytes. *PLoS ONE* 4: e8251.
35. **Larsen AP, Steffensen AB, Grunnet M, Olesen SP** (2011) Extracellular potassium inhibits Kv7.1 potassium channels by stabilizing an inactivated state. *Biophys J* 101: 818–827.
36. **Yeung SYM, Lange W, Schwake M, Greenwood IA** (2008a) Expression profile and characterisation of a truncated KCNQ5 splice variant. *Biochem Biophys Res Commun* 371: 741–746.
37. **Su TR, Chen CH, Huang SJ, Lee CY, Su MC, et al.** (2009) Functional study of the effect of phosphatase inhibitors on KCNQ4 channels expressed in *Xenopus* oocytes. *Acta Pharmacol Sin* 30: 1220–1226.
38. **Soh H, Tzingounis AV** (2010) The specific slow afterhyperpolarization inhibitor UCL2077 is a subtype-selective blocker of the epilepsy associated KCNQ channels. *Mol Pharmacol* 78: 1088–1095.
39. **Brueggemann LI, Mackie AR, Martin JL, Cribbs LL, Byron KL** (2011) Diclofenac distinguishes among homomeric and heteromeric potassium channels composed of KCNQ4 and KCNQ5 subunits. *Mol Pharmacol* 79: 10–23.
40. **Lerche C, Scherer CR, Seebohm G, Derst C, Wei AD, et al.** (2000) Molecular cloning and functional expression of KCNQ5, a potassium channel subunit that may contribute to neuronal M-current diversity. *J Biol Chem* 275: 22395–22400.
41. **Yeung S, Schwake M, Pucovsk V, Greenwood I** (2008b) Bimodal effects of the Kv7 channel activator retigabine on vascular K⁺ currents. *Br J Pharmacol* 155: 62–72.
42. **Roura-Ferrer M, Etxebarria A, Sol L, Oliveras A, Comes N, et al.** (2009) Functional implications of KCNE subunit expression for the Kv7.5 (KCNQ5) channel. *Cell Physiol Biochem* 24: 325–334.
43. **Zhang S, Kehl SJ, Fedida D** (2003) Modulation of human ether-à-go-go-related K⁺ (HERG) channel inactivation by Cs⁺ and K⁺. *J Physiol* 548: 691–702.
44. **Wang SY, Yoshino M, Sui JL, Wakui M, Kao PN, et al.** (1998) Potassium currents in freshly dissociated uterine myocytes from nonpregnant and late-pregnant rats. *J Gen Physiol* 112: 737–756.
45. **Varró A, Baczkó I** (2011) Cardiac ventricular repolarization reserve: a principle for understanding drug-related proarrhythmic risk. *Br J Pharmacol* 164(1):14–36.
46. **Chiesa N, Rosati B, Arcangeli A, Olivetto M, Wanke E** (1997) A novel role for HERG K⁺ channels: spike-frequency adaptation. *J Physiol* 501: 313–318.
47. **Sharp GC, Saunders PTK, Norman JE** (2013) Computer models to study uterine activation at labour. *Mol Hum Reprod* 19:711–717.
48. **Pervolaraki E, Holden AV** (2013) Spatiotemporal patterning of uterine excitation patterns in human labour. *Biosystems* 112:63–72.
49. **Taggart MJ, Wray S** (1998) Hypoxia and smooth muscle function: key regulatory events during metabolic stress. *J Physiol* 509: 315–325.
50. **Young RC, Goloman G** (2013) Phasic oscillations of extracellular potassium (K_o) in pregnant rat myometrium. *PLoS ONE* 8(5):e65110.
51. **Goldbeter A, Gérard C, Gonze D, Leloup JC, Dupont G** (2012) Systems biology of cellular rhythms. *FEBS Lett* 586: 2955–2965.
52. **Hamby DM** (1994) A review of techniques for parameter sensitivity analysis of environmental models. *Environmental Monitoring and Assessment* 32: 135–154.
53. **Ermentrout GB** (2002) *Simulating, analysing, and animating dynamical systems: a guide to XPPAUT for researchers and students*. Philadelphia, US: society for Industrial and Applied Mathematics.